Assessing the quality of the random phase approximation for lattice constants and atomization energies of solids

Judith Harl,* Laurids Schimka, and Georg Kresse
Faculty of Physics, Center for Computational Materials Science, Universität Wien, Sensengasse 8/12, A-1090 Wien, Austria
(Received 30 November 2009; revised manuscript received 28 January 2010; published 17 March 2010)

We present lattice constants, bulk moduli, and atomization energies of solids using the correlation energy evaluated within the adiabatic connection fluctuation-dissipation framework and applying the random-phase approximation. Recently, we have shown [Phys. Rev. Lett. **103**, 056401 (2009)] that geometrical properties and heats of formation are well described within this approximation. We extend this study to a larger set of materials and focus on the treatment of metals and the effect introduced by the frozen-core approximation.

DOI: 10.1103/PhysRevB.81.115126 PACS number(s): 71.10.−w, 71.15.−m, 61.50.Lt

I. INTRODUCTION

Density functional theory (DFT) in the formulation of Kohn and Sham (KS) (Ref. 1) provides an efficient way to evaluate a wide range of ground-state properties. This high efficiency is realized by mapping the problem of interacting electrons onto a reference system of noninteracting electrons moving in an effective local potential. The complexity of the many-body problem is thereby transferred to the description of the exchange-correlation energy functional $E_{xc}[n]$, which can be proven to be a unique functional of the electronic ground-state density. The most widely used approximations to E_{xc} are the local density approximation (LDA) (Ref. 1) and the generalized gradient approximation (GGA), the Perdew-Burke-Ernzerhof (PBE) (Ref. 2) functional being a popular representative of the latter. Within the LDA and GGA the exchange-correlation energy of the considered system is approximated locally by the exchange-correlation energy of the uniform electron gas (UEG) (in the case of the LDA) or semilocally (GGA) by taking also the density gradient into account. Despite the remarkable success of LDA/GGA based KS theory, the locality of the approximation leads to systematic errors. Among them is the self-interaction error and the inaccurate description of negative ions due to the exponential (instead of $1/r$) decay of the LDA/GGA exchange-correlation potential far away from the nucleus. These failures can be cured by the inclusion of exact exchange. Nevertheless, as a large part of the LDA/GGA accuracy relies on the cancellation of errors in the exchange and correlation energy, combining exact exchange and LDA/GGA correlation generally worsens the performance.[3] Hybrid functionals such as PBE0 (Ref. 4) add only a part of exact exchange, which seems to be a good compromise for a wide range of systems[4–7] but obviously does not restore the correct $1/r$ decay in vacuum. Furthermore, a consistent treatment of long-range van der Waals (vdW) dispersion forces, which require the accurate description of the long-range part of the correlation energy, remains out of scope for hybrid functionals.

Alternatively, quantum chemical methods such as Møller-Plesset perturbation theory (e.g., MP2) or coupled cluster methods can be applied. These methods are widely used for molecular systems, but constitute a computational challenge for solids. Recently MP2 has been implemented for periodic systems[8–10] and coupled cluster methods can be applied to solids using an incremental method,[11] but applications are restricted to very small systems because of the large computational complexity and demand of these methods.

An alternative and fairly efficient framework is the adiabatic connection fluctuation-dissipation (ACFD) theory,[12–14] which in principle allows for an exact evaluation of the exchange-correlation energy within DFT. Within the ACFD framework, the total energy of a system is reformulated as a sum of the kinetic energy of the noninteracting Kohn-Sham (KS) system, T_{KS}, the energy arising from the interaction with the ionic background $E_{\text{ion-el}}$, and the Hartree and exchange-correlation energy E_{Hxc}. The latter equals the integral over the ground-state expectation value of the electron-electron interaction operator $\hat{V}_{ee}=1/2\Sigma_{i,j\neq i}e^2/|\mathbf{r}_i-\mathbf{r}_j|=:1/2\Sigma_{i,j\neq i}v(\mathbf{r}_i-\mathbf{r}_j)$, when adiabatically switching from the KS system of noninteracting electrons ($\lambda=0$) to the system of fully Coulomb interacting electrons ($\lambda=1$)

$$E = T_{KS} + E_{\text{ion-el}} + \underbrace{\int_0^1 d\lambda \langle \Psi(\lambda)|\hat{V}_{ee}|\Psi(\lambda)\rangle}_{E_{Hxc}}. \tag{1}$$

The many-electron wave function $\Psi(\lambda)$ represents the ground state of the Hamiltonian $\hat{H}=\hat{T}+\Sigma_i v^\lambda(\mathbf{r}_i)+\lambda\hat{V}_{ee}$, where the local potential v^λ is chosen as to fix the electron density to the one of the fully interacting system. For the KS system ($\lambda=0$), the ground-state wave function is a single Slater determinant of one-electron orbitals $\Psi^{KS}=S(\{\psi_i^{KS}\})$. Due to the fluctuation-dissipation theorem, E_{Hxc} can be written as

$$E_{Hxc} = E_H[n] + E_x[\{\psi_i^{KS}\}] \underbrace{- \int_0^1 d\lambda \int_0^\infty \frac{d\omega}{2\pi} \text{Tr}\{v[\chi^\lambda(i\omega) - \chi^{KS}(i\omega)]\}}_{E_c}, \tag{2}$$

making use of the response function of the interacting system, $\chi^\lambda(i\omega)$, and of the noninteracting KS system, $\chi^{KS}(i\omega)$ at imaginary frequencies. The exchange energy E_x is given by the exact exchange energy expression evaluated at the "true" KS orbitals, in practice, at KS-LDA or KS-GGA orbitals. In

the present case, the trace Tr and the matrices χ^{KS} and χ^{λ} are evaluated in a plane wave basis set.

A relationship between the linear response function of the interacting system with the coupling strength λ and the independent particle KS response function χ^{KS} can be established by a Dyson-like equation,[15,16]

$$\chi^{\lambda}(\mathbf{q},i\omega)^{-1} = \chi^{KS}(\mathbf{q},i\omega)^{-1} - [\lambda\nu(\mathbf{q}) + f_{xc}^{\lambda}(\mathbf{q},i\omega)]. \quad (3)$$

The exchange-correlation kernel $f_{xc}^{\lambda}(\mathbf{q},i\omega)$ is neglected in the following $[f_{xc}^{\lambda}(\mathbf{q},i\omega)=0]$, an approximation which is generally referred to as random phase approximation (RPA). In the context of many-body perturbation theory, the RPA correlation energy equals the Klein energy functional applying the GW approximation.[17] The expansion of the RPA correlation energy for a weak electron-electron interaction ($\lambda \ll 1$) corresponds to the direct-term of the MP2 energy (see e.g., Ref. 9). However, in contrast to the MP2 correlation energy, the RPA correlation energy of metals is finite and errors are comparable to the ones obtained for insulators. The relation between RPA and coupled cluster theory has been hinted at by Freeman more than 40 years ago[18] and has been established recently by Scuseria *et al.*[19]

The RPA is known to describe the long-range dependence of the correlation energy well,[14,20] but absolute correlation energies can deviate from the correct values by 30–40 % (see, e.g., Ref. 21 for the correlation energy of the UEG and Ref. 22 for total correlation energies of atoms), the dominant error being related to the neglect of exchange like diagrams, comparable to the exchange like term in MP2.[18,23] The large RPA error in the total correlation energy inspired the introduction of a correction term given by, e.g.,

$$E_c^{\mathrm{corr,LDA}} = \int d^3r n(\mathbf{r})(e_c^{\mathrm{QMC}}[n] - e_c^{\mathrm{RPA}}[n]), \quad (4)$$

where e_c^{QMC} and e_c^{RPA} are the exact (quantum Monte Carlo) and RPA correlation energies per electron of the UEG, so that Eq. (4) per definition cancels the RPA short-range correlation error for the UEG.[20] The resulting method, which is referred to as RPA+, improves the total correlation energies of atoms,[22] but unfortunately does not outperform the uncorrected RPA for atomization energies of molecules.[24]

The RPA has been applied to jellium bulk, jellium surfaces, and slabs[14,25–30] since more than 40 years, but realistic molecular,[22,31–40] solid,[38,41–46] and surface[47,48] systems have only been considered recently. This is related to the fact that the RPA correlation energy requires the evaluation of the response function and, therefore, usually the inclusion of a large number of unoccupied states. Hence, RPA calculations are more demanding than DFT calculations and scale worse with system size. Although the use of unoccupied states can be circumvented by using density functional perturbation theory as recently applied in Refs. 44 and 45, density functional perturbation theory does not reduce the complexity (scaling). The large computational demand has postponed a systematic assessment of the quality of the RPA for lattice constants, bulk moduli, and atomization energies. Only recently,[46] we have shown that the RPA provides a very good description of lattice constants for covalently, ionic, metallic, as well as van der Waals bonded systems.[38] In the present work, we extend the study to a larger number of systems (additionally including Ge, AlN, AlAs, GaN, GaP, GaAs, InP, InAs, and InSb), and we will provide technical details about the treatment of metals and the accuracy of the frozen-core approximation.

This paper is organized as follows. In Sec. II, technical details concerning the implementation of the RPA routines and the settings chosen in this work will be discussed. In Sec. II D, RPA calculations for metals will be focused on and Sec. II F deals with the quality of the frozen-core approximation. Lattice constants and bulk moduli are presented in Sec. III A, atomization energies in Sec. III B. In Sec. IV, we will discuss our results in the context of possible improvements of the RPA correlation energy.

II. TECHNICAL DETAILS

A. Total energy and response function

The RPA-ACFD routines have been implemented in the Vienna Ab initio Simulation Package (VASP).[49,50] Within this plane wave basis set code the interaction between the ionic cores and the valence electrons is described by the projector-augmented wave (PAW) (Ref. 51) method in the implementation of Kresse and Joubert.[52] For details related to the calculation of the exact exchange energy we refer to Refs. 5 and 6. Technical details concerning the optical routines within VASP are presented in Refs. 53 and 54. For the calculation of the response function, the all-electron charge density is restored accurately on the plane wave grid. The implementation of the RPA correlation energy in VASP has been more extensively discussed in Ref. 38.

In the following sections, we will present lattice constants and atomization energies of solids. To this end, we evaluate the total energy of the system as given by

$$E = \underbrace{T_{KS} + E_{\text{ion-e}} + E_H + E_x}_{E_{\mathrm{EXX}}} + E_c^{\mathrm{RPA}}. \quad (5)$$

The total energy without the RPA correlation energy equals the Hartree-Fock energy expression evaluated for KS orbitals, and is therefore referred to as exact exchange (EXX) energy E_{EXX}. For most materials, we have chosen to converge E_{EXX} and the correlation energy E_c^{RPA} independently.

The ACFD correlation energy is defined by Eq. (2). If the response function of the λ-interacting system is approximated within the RPA, as done in the present work, the integration over the coupling constant λ in Eq. (2) can be performed analytically and the RPA-ACFD correlation energy becomes[55]

$$E_c^{\mathrm{RPA}} = \int_0^{\infty} \frac{d\omega}{2\pi} \mathrm{Tr}\{\ln[1 - \nu\chi^{KS}(i\omega)] + \nu\chi^{KS}(i\omega)\}. \quad (6)$$

In reciprocal space, the trace Tr is calculated as

$$\mathrm{Tr}\{AB\} := \sum_{\mathbf{q}\in BZ} g_{\mathbf{q}} \sum_{\substack{|\mathbf{G}+\mathbf{q}|<G^{\chi}_{\mathrm{cut}} \\ |\mathbf{G}'+\mathbf{q}|<G^{\chi}_{\mathrm{cut}}}} A_{\mathbf{G}\mathbf{G}'}(\mathbf{q}) B_{\mathbf{G}'\mathbf{G}}(\mathbf{q}). \quad (7)$$

The k-point weights $g_{\mathbf{q}}$ are chosen to generate the correct BZ sampling for a given set of k points, and they sum to 1. The response function and other matrices are expanded in a plane wave basis set, where all plane waves up to a maximum reciprocal lattice vector G^{χ}_{cut} are included. The dependence of the correlation energy on G^{χ}_{cut} is discussed in Sec. II C. Equation (6) is evaluated using the identity $\mathrm{Tr}\{\ln[1-\nu\chi]+\nu\chi\} = \mathrm{Tr}\{\ln[1-\nu^{1/2}\chi\nu^{1/2}]+\nu^{1/2}\chi\nu^{1/2}\} = \Sigma_i \ln(1-\bar{\varepsilon}_i)+\bar{\varepsilon}_i$, where $\bar{\varepsilon}_i$ are the eigenvalues of the Hermitian matrix $\nu^{1/2}\chi\nu^{1/2}$.

The independent-particle response function χ^{KS} (the response of the KS system) at imaginary frequencies is given by the expression of Adler[56] and Wiser[57]

$$\chi^{KS}_{\mathbf{G}\mathbf{G}'}(\mathbf{q},i\omega) = \frac{1}{V}\sum_{nn'\mathbf{k}} 2g_{\mathbf{k}}(f_{n'\mathbf{k}+\mathbf{q}} - f_{n\mathbf{k}}) \times \frac{\langle \psi_{n'\mathbf{k}+\mathbf{q}} | e^{i(\mathbf{q}+\mathbf{G})\mathbf{r}} | \psi_{n\mathbf{k}} \rangle \langle \psi_{n\mathbf{k}} | e^{-i(\mathbf{q}+\mathbf{G}')\mathbf{r}'} | \psi_{n'\mathbf{k}+\mathbf{q}} \rangle}{\epsilon_{n'\mathbf{k}+\mathbf{q}} - \epsilon_{n\mathbf{k}} - i\omega}, \quad (8)$$

where $\psi_{n\mathbf{k}}$ and $\epsilon_{n\mathbf{k}}$ are the KS one-electron orbitals and energies of state n and crystal momentum vector $\mathbf{k}$, which lies within the first Brillouin zone of the primitive cell with volume V. The summation is performed over all occupied and unoccupied orbitals n and n', and the occupation number is described by the function $f_{n\mathbf{k}}$, which is 1 if the respective orbital is occupied and 0 otherwise.

Since the λ integration can be performed analytically, only the frequency integration and the dependence of the correlation energy on the maximal reciprocal lattice vector G^{χ}_{cut} [see Eq. (7) and Sec. II C] are left for discussion.

Because the response function is evaluated at imaginary frequencies, the integrand in Eq. (6) is a smooth function with respect to the frequency and the frequency integration is therefore fairly unproblematic. We use a Gauss-Legendre integration and the weighting function is chosen to decay exponentially for large frequencies. We set the maximal frequency for all considered materials to 800 eV. With 16 frequency points, the error in the total correlation energy introduced by the discretized frequency integration is throughout smaller than 1–2 meV for solids and 5–10 meV for atoms.

The actual calculation of the RPA correlation energy proceeds in three steps. (i) A standard self-consistent KS-DFT calculation with a plane wave energy-cutoff E_{cut} is performed. Except for test calculations, we use the GGA parameterization by Perdew-Burke-Ernzerhof (PBE). (ii) In a final KS-DFT step, the one-electron wave functions and eigenenergies of all unoccupied (virtual) orbitals spanned by the plane wave basis set are evaluated by an exact diagonalization of the previously determined self-consistent KS Hamiltonian. Hence, the number of filled and empty orbitals is equivalent to the number of plane waves, which is, in turn, restricted by the energy cutoff E_{cut}. (iii) In the third step, the independent-particle KS response function $\chi^{KS}(\mathbf{q},i\omega)$ is evaluated from the KS orbitals and eigenenergies calculated in step (ii) and the RPA correlation energy is evaluated via Eq. (6).

B. PAW Potentials

As a large number of unoccupied states is required for the calculation of the RPA correlation energy, we use special PAW potentials throughout this work. These potentials are constructed to describe the scattering properties of the atoms very accurately up to ≈10 Ry above the vacuum level by choosing additional reference energies and partial waves situated above the vacuum level (for more details see Ref. 54). In Table I, the chosen settings for the potentials used in the present work are summarized. For the third period elements Na, Al, Si, P, Cl, as well as fluor, d-projectors and partial waves have been included in order to guarantee an accurate treatment of the unoccupied d states. For the same reason, f projectors have been included for Ag, Rh, Pd, and Sb.

All potentials used in this work have been constructed for the LDA. Also the PBE lattice constants and atomization energies presented in Secs. III A and III B have been evaluated using these potentials, which leads to slight discrepancies with the PBE values in Ref. 58. The influence of evaluating core-valence contributions using frozen LDA instead of PBE core states is however small, being largest for diamond (0.14% in the lattice constant). Extensive tests for transferring PAW potentials constructed for one specific exchange-correlation potential (e.g., LDA) to another exchange-correlation potential (e.g., PBE) can be found in Ref. 59.

In order to test the quality of the frozen-core approximation, additional PAW potentials that treat deeper lying states as valence have been generated for some elements (Na, Al, Si, Cu, Ga). These potentials are labeled by subscripts denoting the states which have additionally been included in the valence. For Na, Al, and Si, potentials "unfreezing" the 2s and 2p states have been constructed (Na_{2s2p}, Al_{2s2p}, Si_{2s2p}), for Cu the 3p states (Cu_{3p}) and for Ga the 3s and 3p (Ga_{3s3p}) states have been included in the valence. The effect that is caused by explicitly treating these core states is presented in Sec. II F.

C. Basis set convergence—Auxilary basis set for response function

The maximal reciprocal lattice vector in Eq. (7) is defined via the requirement that $\hbar^2/(2m)(\mathbf{G}+\mathbf{q})^2 < E^{\chi}_{\mathrm{cut}} =: \hbar^2/(2m)(G^{\chi}_{\mathrm{cut}})^2$ and E^{χ}_{cut} is provided as an input parameter. The dependence of the correlation energy on E^{χ}_{cut} is large and absolute convergence with respect to E^{χ}_{cut} can hardly be achieved. But we found that the RPA correlation energy of the homogenous electron gas depends on E^{χ}_{cut} as[38]

$$E_c(E^{\chi}_{\mathrm{cut}}) = E_c^{\infty} + \frac{A}{(G^{\chi}_{\mathrm{cut}})^3} = E_c^{\infty} + \frac{A'}{(E^{\chi}_{\mathrm{cut}})^{3/2}}, \quad (9)$$

with A and A', respectively, being constants. Similar to the molecules and the rare gas solids considered in Ref. 38, this

TABLE I. PAW potentials used in the present work. In the second column, the states treated as valence are indicated. As local potential, a pseudopotential was generated for the states indicated in the column "local." For some elements (Li, Mg, Cu, Rh, Pd, Ag, and Sb), the local potential was generated by replacing the AE potential by a soft potential within the cutoff radius r_{loc} (a.u.), which, in these cases, is provided in the "local" column. The number of partial waves and projectors for different angular momentum numbers l is specified in columns 4–7. The energy cutoff E_{cut} refers to the standard energy cutoff for DFT calculations, the energy cutoffs applied in the EXX and RPA calculations are summarized in Table III.

	Valence	Local	s	p	d	f	E_{cut} (eV)
Li	$1s2s$	1.0	3	2			433
C	$2s2p$	$3d$	2	2			414
N	$2s2p$	$3d$	2	2			420
O	$2s2p$	$3d$	2	2			414
F	$2s2p$	$4f$	3	3	2		487
Na	$3s$	$4f$	2	2	2		82
Na_{2s2p}	$2s2p3s$	$4f$	3	3	2		260
Mg	$2s2p3s$	1.5	3	3	1		470
Al	$3s3p$	$4f$	2	2	2		241
Al_{2s2p}	$2s2p3s3p$	$4f$	3	3	2		411
Si	$3s3p$	$4f$	2	2	2		246
Si_{2s2p}	$2s2p3s3p$	$4f$	3	3	2		475
P	$3s3p$	$4f$	2	2	2		255
Cl	$3s3p$	$4f$	2	2	2		262
Cu	$3d4s$	1.5	2	2	2		417
Cu_{3p}	$3p3d4s$	1.5	2	2	2		467
Ga	$3d4s4p$	$4f$	2	3	3		370
Ga_{3s3p}	$3s3p3d4s4p$	$4f$	3	3	3		503
Ge	$3d4s4p$	$4f$	2	2	2		310
As	$4s4p$	$4f$	2	2	1		209
Rh	$4d5s$	1.6	2	2	2	2	247
Pd	$4d5s$	1.6	2	2	2	2	250
Ag	$4d5s$	1.4	2	2	2	2	250
In	$4d5s5p$	$5f$	2	2	3		279
Sb	$4d5s5p$	1.6	2	2	3	2	263

behavior is observed for all solids in this work, as long as core states are not treated as valence. If core states are explicitly considered, only atomization energies and differences between correlation energies exhibit a behavior according to Eq. (9). The dependence of the lattice constant, the bulk modulus, the total correlation energy, and the atomization energy (correlation+EXX energy difference) on E_{cut}^{χ} is presented in Table II for Si, treating only the $3s$ and $3p$ states as valence (top), and including additionally the $2s$ and $2p$ core states in the valence (Si_{2s2p}, bottom). It is obvious that the applied extrapolation procedure is absolutely necessary but remarkably accurate and allows to obtain meV convergence for relative energies and 0.1% precision for lattice constants at moderate settings.

In routine calculations, the correlation energy for $E_{\mathrm{cut}}^{\chi} \rightarrow \infty$ is determined by evaluating the correlation energy for eight values of E_{cut}^{χ} (in steps of 5% of the largest chosen E_{cut}^{χ} value) and applying a linear regression to determine E_c^{∞} and A' in Eq. (9). In the following, the maximum E_{cut}^{χ} is chosen to be between 1/2–2/3 of E_{cut}. To obtain smooth curves for the correlation energy $E_c(E_{\mathrm{cut}}^{\chi})$, we additionally apply a Hann-like window function $\{0.5[1+\cos(x)\}$, which goes from 1 at $0.8E_{\mathrm{cut}}^{\chi}$ to 0 at E_{cut}^{χ}, in order to smoothly cut off the contributions from large G vectors in the response function.

D. *k*-point convergence

In this section, we discuss the k-point convergence of the EXX and RPA correlation energy for insulators, semiconductors, and metals. All calculations were performed using Γ-centered Monkhorst-Pack k-point grids.

1. Exact exchange energy

In the Hartree-Fock case, the exchange energy is given by[60,61]

TABLE II. Lattice constant a (Å), bulk modulus B (GPa), absolute bulk and atomic correlation energy E_c (eV/atom), and atomization energy ΔE (eV/atom) evaluated using different energy cutoffs for the response function E_{cut}^{χ} (eV), as well as interpolating between values of E_{cut}^{χ} using relation (9).

E_{cut}^{χ}	a	B	E_c^{bulk}	E_c^{atom}	ΔE
			Si		
142	5.463	95.1	−16.216	−4.331	4.309
173	5.455	95.9	−16.292	−4.386	4.330
200	5.451	96.4	−16.336	−4.418	4.342
142–173	5.432	98.6	−16.518	−4.549	4.393
173–200	5.431	98.6	−16.517	−4.547	4.394
142–200	5.432	98.6	−16.517	−4.548	4.393
			Si_{2s2p}		
213	5.444	96.7	−17.365	−6.547	4.331
246	5.443	96.8	−17.734	−6.915	4.333
300	5.441	97.0	−18.276	−7.455	4.334
213–246	5.438	97.5	−19.239	−8.411	4.341
246–300	5.438	97.4	−19.870	−9.046	4.337
213–300	5.438	97.4	−19.638	−8.813	4.338

$$E_x = -e^2 \sum_{\mathbf{q}} \sum_{\mathbf{k}nn'} f_{n\mathbf{k}} g_{\mathbf{k}} f_{n'\mathbf{k}+\mathbf{q}} g_{\mathbf{k}+\mathbf{q}} \times \int\int d^3r d^3r' \frac{\psi_{n\mathbf{k}}^*(\mathbf{r})\psi_{n'\mathbf{k}+\mathbf{q}}(\mathbf{r})\psi_{n'\mathbf{k}+\mathbf{q}}^*(\mathbf{r}')\psi_{n\mathbf{k}}(\mathbf{r}')}{|\mathbf{r}-\mathbf{r}'|}. \tag{10}$$

However, within the ACFD framework, the "exchange" energy is usually defined as the exchange-correlation energy at zero coupling strength,

$$E_x^{\mathrm{EXX}} = -\frac{e^2}{2}\int d^3r d^3r' \frac{1}{|\mathbf{r}-\mathbf{r}'|} \times \left[n(\mathbf{r})\delta(\mathbf{r}-\mathbf{r}') + \frac{1}{\pi}\int_0^\infty d\omega \chi^{KS}(\mathbf{r},\mathbf{r}',i\omega) \right]. \tag{11}$$

Inserting the independent-particle response function χ^{KS} [Eq. (8)] leads to an alternative definition of the exchange energy,

$$E_x^{\mathrm{EXX}} = -e^2 \sum_{\mathbf{q}} \sum_{\mathbf{k}nn'} f_{n\mathbf{k}} g_{\mathbf{k}} g_{\mathbf{k}+\mathbf{q}} \times \left(1 - \frac{2}{\pi}\int_0^\infty d\omega \frac{(\epsilon_{n'\mathbf{k}+\mathbf{q}} - \epsilon_{n\mathbf{k}})}{(\epsilon_{n'\mathbf{k}+\mathbf{q}} - \epsilon_{n\mathbf{k}})^2 + \omega^2} \right) \times \int\int d^3r d^3r' \frac{\psi_{n\mathbf{k}}^*(\mathbf{r})\psi_{n'\mathbf{k}+\mathbf{q}}(\mathbf{r})\psi_{n'\mathbf{k}+\mathbf{q}}^*(\mathbf{r}')\psi_{n\mathbf{k}}(\mathbf{r}')}{|\mathbf{r}-\mathbf{r}'|}. \tag{12}$$

The frequency integration can be performed analytically, yielding $\pi/2\ \mathrm{Sgn}(\epsilon_{n'\mathbf{k}+\mathbf{q}} - \epsilon_{n\mathbf{k}})$, but in practice, Eq. (12) is applied as it stands in order to guarantee full compatibility with the evaluation of the RPA correlation energy. For insulators and semiconductors with integer occupancies, Eq. (12) obviously equals Eq. (10). However, for partially filled orbitals, Eq. (12) involves only a single occupancy, instead of the symmetric two occupancies in Eq. (10). We will show below that Eq. (12) is the preferred definition for systems with fractionally filled states within the RPA framework. As pointed out in Ref. 61, the integrand for E_{xc} at zero coupling strength [Eq. (12)] is not equivalent to the Hartree-Fock exchange energy, since it possesses an additional static correlation contribution. Mori-Sánchez, Cohen, and Yang came to a similar conclusion recently.[39] They "generalized" time dependent DFT, specifically the Casida equation,[62] to systems with partially filled states. In their case, the correlation energy possesses an additional contribution as well that, after some manipulation, turns out to be equivalent to the difference between Eq. (10) and Eq. (12).[39] We furthermore note that their seemingly "new" derivation for TD-DFT with partially filled states is fully compatible with the formulation of Adler[56] and Wiser[57] [Eq. (8)], and hence fully compatible with our present calculations.

Despite the fact that the difference between Eqs. (10) and (12) might be attributed to static correlation, there is also a simple, physically appealing interpretation of the exchange energy defined according to Eq. (12). It might be interpreted as the nonlocal exchange energy in the *grand canonical* ensemble with fluctuating electron numbers. Assuming that the ground state is spanned by a set of one-electron orbitals $\{\psi_m, m=1,N\}$ with increasing one electron energies, the many-electron ground-state wave function for a system with n electrons, Ψ_n is given by the Slater determinant $\Psi_n = S(\{\psi_m, m=1,n\})$. The probability to find the system in this state is f_n, where the occupancies observe $f_{n-1} > f_n, \forall n$. Then the exchange energy for that many-electron state is obviously given by $E_x(\Psi_n)$, and the total exchange energy is given by $E_x^{\mathrm{EXX}} = \Sigma_n f_n E_x(\Psi_n)$, which is equivalent to Eq. (12).

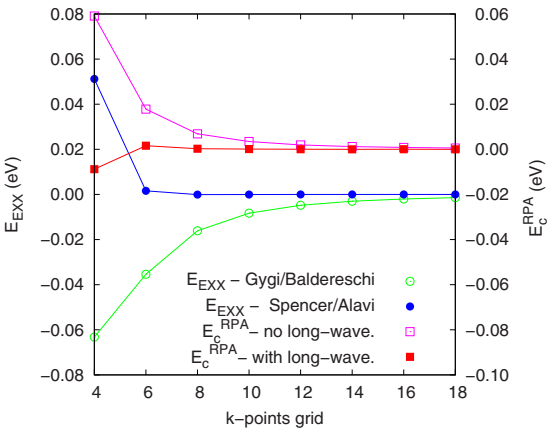

FIG. 1. (Color online) *k*-point convergence for diamond including and excluding the long-wavelength response function when evaluating the RPA correlation energy. The EXX energies ($E-E_c^{\mathrm{RPA}}$) have been evaluated using the Gygi/Baldereschi (Ref. 63) (excludes the long-wavelength response in the exchange) and the Spencer/Alavi (Ref. 64) scheme (includes long-wavelength response in the exchange).

We note that the kinetic energy and the polarizability in the formulation of Adler and Wiser are consistent with this interpretation. In our present implementation, only the Hartree energy is calculated inconsistently with the Grand canonical interpretation. But since convergence of the Hartree energy with respect to the k points is very fast for metallic systems, we did not find this to be a major issue here. However, it is conceivable that a consistent definition should be applied for defect levels of atoms and molecules with partial occupancies.

2. Insulators

To deal with the singularity of the Coulomb kernel $\nu_{\mathbf{G},\mathbf{G}'}(\mathbf{q})=4\pi e^2/|\mathbf{q}+\mathbf{G}|^2\delta_{\mathbf{G},\mathbf{G}'}$ for $\mathbf{G}=0$ and $\mathbf{q}\to 0$ in the exchange energy, two distinct schemes can be found in literature. The first one was suggested by Gygi and Baldereschi[63] and essentially attempts to deal with the singularity of the first term in Eq. (11), but entirely neglects the long-wavelength contribution of the second term. The second scheme has been suggested by Spencer and Alavi.[64] It introduces a finite cutoff radius for the Coulomb kernel. This method becomes exact if the cutoff radius in the Coulomb kernel is twice as large as the maximal spatial extent of all Wannier functions, which is easily recognized by writing the exchange energy in Eq. (10) or Eq. (12) in a basis of Wannier orbitals.

Figure 1 shows the EXX energy and correlation energy for diamond as a function of the number of k points N_k, where N_k is the number of points in one direction of the Brillouin zone. In the Spencer/Alavi scheme the exchange energy converges exponentially to the correct solution, and the error is essentially zero for $N_k=6$ corresponding to a Coulomb cutoff of $r=7.95$ Å. For the Gygi and Baldereschi scheme, the error is proportional to $1/(N_k)^3$, hence proportional to the reciprocal space volume around the Γ point. The reason for this slow convergence is that this scheme neglects the $\mathbf{q}\to 0$, $\mathbf{G}=\mathbf{G}'=0$ contributions from the second term in Eq. (11). After Fourier transformation to reciprocal space this contributions becomes proportional to (the indices $\mathbf{G}=0$ and $\mathbf{G}'=0$ have been dropped for brevity)

$$-\lim_{\mathbf{q}\to 0}\int_0^\infty \frac{d\omega}{2\pi}\nu(\mathbf{q})\chi(\mathbf{q},i\omega) \tag{13}$$

times the reciprocal space volume around the Γ point, which is proportional to $1/(N_k)^3$. By Taylor expansion of the orbitals around $\mathbf{q}=0$, the singularity in the Coulomb kernel can be lifted, and hence the long-wavelength contribution becomes finite for systems with a band gap (see Ref. 53 for details in the PAW case). However, this contribution has not been included in Fig. 1.

A related issue is the treatment of the long-wavelength $\mathbf{q}\to 0$, $\mathbf{G}=\mathbf{G}'=0$ contribution to the correlation energy in the RPA, which also involves products of the polarizability with the Coulomb kernel,

$$\lim_{\mathbf{q}\to 0}\int_0^\infty \frac{d\omega}{2\pi}\{\ln[1-\nu(\mathbf{q})\chi(\mathbf{q},i\omega)]+\nu(\mathbf{q})\chi(\mathbf{q},i\omega)\}. \tag{14}$$

This contribution can be also evaluated in analogy to Ref. 53 for the PAW case. In Fig. 1, the RPA correlation energy is shown versus the chosen k-point grid without (empty squares) and including (filled squares) the long-wavelength part of the correlation energy. Clearly, inclusion of the long-wavelength contribution speeds up the k-point convergence significantly. If $\lim_{\mathbf{q}\to 0}\nu(\mathbf{q})\chi(\mathbf{q},i\omega)$ is not evaluated, the best choice is *to neglect the contribution both in the exact exchange and in the correlation energy*, since

$$\ln[1-\nu(\mathbf{q})\chi(\mathbf{q},i\omega)] \ll -\nu(\mathbf{q})\chi(\mathbf{q},i\omega). \tag{15}$$

In this case, the Gygi and Baldereschi scheme should be applied. This is also visible in Fig. 1, where the sum of EXX(Gygi/Baldereschi) and the correlation energy without the $\mathbf{q}\to 0$ contribution converges fairly rapidly, but still slower than if the $\mathbf{q}\to 0$ contribution is taken into account.

In practice, for insulators and semiconductors, we converge the exchange and correlation separately. To avoid any tedious convergence tests, a denser k-point grid is used for the computationally cheap exchange, whereas the RPA correlation energy is evaluated using a coarser grid. Usually, accurate lattice constants (errors $<0.1\%$) can be obtained using a $4\times4\times4$ k-point grid (16 k points in the IBZ) for RPA, however, converged atomization energies require a slightly denser grid of $6\times6\times6$ k points (29 in IBZ).

3. Metals: Singular contributions

For metals, k-point convergence of the EXX and the RPA correlation energy is more difficult to attain than for insulators. The main difference between metals and insulators is that, whereas for systems with a band gap the polarizability vanishes for $\mathbf{q}\to 0$, for gap less systems it takes on a finite value. This contribution mostly arises from transitions within one and the same band (intraband transitions or Drude term). As a result $\nu(\mathbf{q})\chi(\mathbf{q},i\omega)$ becomes singular at $\omega=0$ and $\mathbf{q}=0$ diverging like

$$\begin{cases} -\omega_{PL}^2/\omega^2 & \text{for } \mathbf{q}=0 \\ q_{TF}^2/q^2 & \text{for } \omega=0,\ \mathbf{q} \text{ small,} \end{cases}$$

where ω_{PL} is the plasma frequency and q_{TF} the Thomas-Fermi wave vector.

Furthermore, for the EXX, the Spencer/Alavi scheme is not applicable, since it relies on a fast (exponential) decay of the Wannier functions, but in metals the Wannier functions are long ranged and decay only algebraically. As a result, the Gygi and Baldereschi scheme is generally found to yield faster convergences. But even then, convergence of the EXX energy with the number of k points N_k is much slower than mentioned in the previous section for insulators and semiconductors, i.e., $1/(N_k)^2$ instead of $1/(N_k)^3$. Matter of fact, this is related to the neglect of the long-wave length limit of the second term in Eq. (11), which obviously diverges for $\mathbf{q}\to 0$ but remains integrable (see next subsection). Also the correlation energy possesses a related integrable singularity at $\mathbf{q}\to 0$.

As we will demonstrate below, reasonable convergence with k points can be obtained by calculating the exact exchange energy and the correlation energy in a fully compatible manner using identical k points. Furthermore, we find empirically that the long-wavelength contributions from the polarizability ($\mathbf{q}=0$) are best entirely neglected in both the exchange and the correlation energy.

In addition to the intraband contributions to the polarizability discussed above, transitions from one to the other band have no lower bound in metals as well. This can result in "problematic" contributions from band-crossings close to the Fermi-energy. In practice, such contributions can lead to a similar divergence of $\nu(\mathbf{q})\chi(\mathbf{q})$ as intraband terms (see Ref. 65). The strength of such transitions depends strongly on the energetic positions of these crossings with respect to the Fermi-level, and it is very sensitive to the k-point grid and volume. Such crossings can also cause a slow convergence of the RPA energy and RPA lattice constants with the number of k points. The problem is again reduced by neglecting the $\mathbf{q}\to 0$ contributions from these transitions in the exchange and correlation energy.

4. Metals: Convergence tests

As a simple test representative of the case without band crossing problems, we consider the k-point convergence of bcc Na. In Fig. 2, the exact exchange energy E_{EXX} of Na evaluated using Eq. (12) (Gygi/Baldereschi scheme), the RPA correlation energy, and the sum of both are plotted versus the number of k points. In the inset, the energy E_{EXX} using Eq. (10) is shown. The dependence of the exchange and correlation energy on the broadening width σ of the smearing function in the Methfessel-Paxton scheme,[66] is considered as well.

Contrary to insulators, where the Gygi and Baldereschi scheme leads to a leading error of the order $1/N_k^3$, the exact exchange energy is found to converge like $1/N_k^2$ for metals. As already mentioned, the increase in the leading error is related to the long-wavelength small frequency behavior of the polarizability $\chi^{KS}(\mathbf{q},i\omega)$ for metals. For the uniform electron gas (UEG), the error can be evaluated exactly inserting

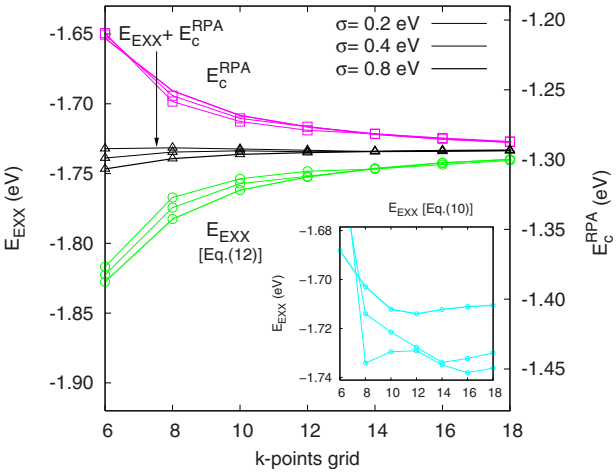

FIG. 2. (Color online) k-point convergence of the exchange energy E_{EXX} and the correlation energy E_c^{RPA}, and total energy ($E_{\mathrm{EXX}}+E_c^{\mathrm{RPA}}$) for Na at the experimental volume. Equation (12) is applied for the exchange, and different broadenings σ are considered. In the inset, the dependence of E_{EXX} is shown for the exchange evaluated using Eq. (10).

the Lindhardt dielectric function in Eq. (11), and carrying out the integration over the frequency and momentum analytically. This yields a contribution $\propto q_{\max}^2 \propto 1/N_k^2$, where $q_{\max}$ is the sphere radius corresponding to the reciprocal space volume around the Γ point.

Whereas the exchange energy E_{EXX} [considering E_x^{EXX} from Eq. (12)] converges from below, the RPA correlation energy converges from above if the long-wavelength part is not taken into account. The sum of the exchange and RPA correlation energy shows the smallest dependence on the k-point grid, because the two errors cancel to a large extent. Unfortunately we were not able to derive an exact analytic formula for the sum of the exchange and correlation energy for the UEG. Nevertheless, Eq. (15) and the presented numerical evidence suggest that the sum is rapidly convergent. This can be also made plausible by the perfect screening properties of metals in the long-wavelength limit, so that the error introduced by the neglect of the $\mathbf{q}\to 0$ contribution to the sum of exchange and correlation is smaller than for either exchange or correlation.

In the inset of Fig. 2, the exchange energy applying definition Eq. (10), E_x, is shown as a function of k points. Not only is the fast convergence of the sum of RPA correlation and exchange not observed, but also the exchange energy is strongly dependent on the broadening width applied in the calculation of the fractional occupancies. This strong dependence on the broadening width indicates that Eq. (10) is not well suited for metals, in general.

The influence of the applied definition for the exchange energy and the effect of interband transitions with very small energy differences is shown for Al and Pd in Fig. 3. For both metals, very good convergence is obtained using Eq. (12) for the EXX energy (E_x^{EXX}) and excluding the long-wavelength part in the RPA correlation energy [Fig. 3(b)]. Use of Eq. (10) [panel (c)] deteriorates convergence significantly, because discontinuities in the energy-volume curve are introduced. Similarly, including the long-wavelength part in the

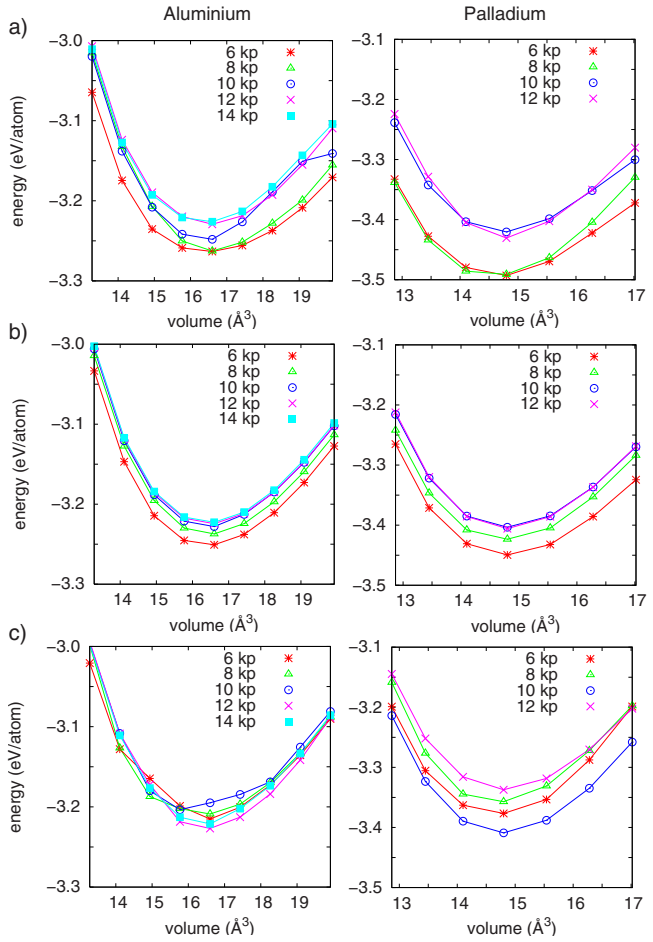

FIG. 3. (Color online) k-point convergence of the RPA correlation plus EXX energy for Al (left side) and Pd (right side), using the same k-point grid for RPA correlation and EXX. The results in panel (a) and panel (b) are both obtained using E_x^{EXX} [Eq. (12)] for the EXX energy, whereas the results in panel (c) were obtained using E_x from Eq. (10). In panel (a) the long-wavelength part of the response function has been included for the evaluation of the RPA correlation energy, in panel (b) and (c) it has been neglected.

correlation only leads to artificial kinks in the energy-volume curve, also slowing convergence with k points.

In summary, fastest convergence for metals is achieved by excluding the long-wavelength part of the exchange and correlation energy, especially for metals with a high electron density at the Fermi level and band crossings close to the Fermi level. Using this approach, reliable lattice constants and atomization energies can be usually obtained for 12 $\times 12 \times 12$ k points.

E. Applied settings

In Table III, the materials considered in the present work are summarized. In addition to the structure, the k-point grid, the energy cutoff chosen for the evaluation of the EXX contribution, E_{EXX}, and the RPA correlation energy, E_c^{RPA}, are tabulated. For the RPA correlation energy, also the largest value chosen for E_{cut}^{χ} is summarized. For the reasons explained in Sec. II D, the same k-point grid has been applied for the EXX and the RPA correlation energy for metals as well as Ge, GaAs, InP, InAs, and InSb, since they are predicted to be metals by PBE/LDA at sufficiently large volumes.

For RPA lattice constants, we aimed at a technical accuracy better than 0.1% for a chosen PAW potential, for the bulk moduli better than 3%. The errors in the EXX lattice constants of metals can be generally larger, since the convergence of the EXX only energy with the number of k points is very slow. We note that similar and very accurate results for the considered properties can often be obtained at much more moderate settings than given in Table III. However, accurate atomization energies generally demand such dense k-point grids and fairly high energy cutoffs. With the settings summarized in Table III, the uncertainty in the atomization energy for a given PAW potential is for most cases smaller than 30 meV. For NaCl, NaF, LiF, LiCl, and MgO, errors in the atomization energy are expected to be slightly larger, since the RPA correlation energies of the Na, Li, Mg atoms converge slowly with respect to the size of the supercell (additional 30 meV). Larger uncertainties are also present for the transition metals Rh and Pd, related to the slow k-point convergence of the bulk energy (additional 20 meV).

F. Influence of core states on the RPA atomization energies and lattice constants

Since RPA calculations constitute a significantly larger computational effort than standard DFT calculations, an all-electron treatment will be hardly possible for routine calculations. The explicit treatment of core states does not only lead to an increase in the number of occupied states, which enter the computational time linearly, it possibly also requires higher Fourier components in the description of the response function (higher energy cutoff E_{cut}^{χ}), since the transition elements between core and unoccupied states involve larger plane wave components. In order to test the validity of the frozen-core approximation for the description of the RPA energy, we evaluate RPA lattice constants and atomization energies, when unfreezing the highest core states of Na, Al, Si, Cu, and Ga (GaP). Independently of the chosen potential, the core-valence contribution to the exact exchange is calculated in any case exactly.[5,54] This is only possible because we use the PAW method and have therefore access to all orbitals (including core states), in contrast to pseudopotential codes.

PBE and RPA lattice constants and atomization energies are summarized in Table IV. Stars label the potentials that have been chosen in the remaining sections. In the final column, the PBE one-particle energy of the highest core state is indicated ($2p$ for Na, Al, and Si, $3p$ for Cu and Ga). Slight changes in the lattice constants and atomization energies are already found on the PBE level. Most of these differences can be traced back to the fact that potentials constructed for LDA atoms have been used in this work and the frozen-core approximation leads to a slight dependence on the underlying potential.

For Na, RPA lattice constants are most strongly influenced by the inclusion of core states (almost 2%). This is not surprising as the $2p$ states are only −25 eV below the Fermi

TABLE III. Settings chosen for the evaluation of the EXX energy and the RPA-ACFD correlation energy. The (different) energy cutoffs E_{cut} (eV) and k-point grids (Γ-centered $k\times k\times k$) used for EXX and RPA calculations are labeled with EXX and RPA, respectively. For systems where RPA results were obtained using the same k-point sampling for the EXX and correlation energy (see Sec. II D), the applied k-point grid is written in bold. Additionally, E_{cut}^{χ}, as chosen for the evaluation of the response function, is specified. The labeling of the potentials follows the one in Table I. Stars indicate the potentials that have been used in the following sections.

Name	Structure	$E_{\mathrm{cut}}^{\mathrm{EXX}}$	k^{EXX}	$E_{\mathrm{cut}}^{\mathrm{RPA}}/E_{\mathrm{cut}}^{\chi}$	k^{RPA}
C*	A4 (diamond)	700	10	460/250	6
Si*	A4 (diamond)	500	10	360/200	6
Si_{2s2p}	A4 (diamond)	1000	10	600/300	6
Ge*	A4 (diamond)	500	10	360/200	**8**
SiC*	B3 (zinc blende)	500	10	460/250	6
AlN*	B3 (zinc blende)	500	10	460/250	6
AlP*	B3 (zinc blende)	360	10	360/200	6
AlAs*	B3 (zinc blende)	360	10	360/200	6
$Ga_{3s3p}N$*	B3 (zinc blende)	800	10	550/300	6
GaP	B3 (zinc blende)	700	10	460/250	6
$Ga_{3s3p}P$*	B3 (zinc blende)	800	10	550/300	6
$Ga_{3s3p}As$*	B3 (zinc blende)	800	10	550/300	**6**
InP*	B3 (zinc blende)	500	10	300/200	**6**
InAs*	B3 (zinc blende)	500	10	300/200	**6**
InSb*	B3 (zinc blende)	500	10	300/200	**6**
MgO*	B1 (rock salt)	900	8	460/250	6
LiF*	B1 (rock salt)	900	8	600/350	6
LiCl*	B1 (rock salt)	700	8	460/250	6
$Na_{2s2p}F$*	B1 (rock salt)	800	8	460/250	6
$Na_{2s2p}Cl$*	B1 (rock salt)	460	8	460/250	6
Na	A2 (bcc)	200	14	200/120	10
Na_{2s2p}^{*}	A2 (bcc)	600	14	360/200	10
Al*	A1 (fcc)	360	20	300/200	**12**
Al_{2s2p}	A1 (fcc)	1000		550/300	**12**
Cu*	A1 (fcc)	600	16	460/250	**12**
Cu_{3p}	A1 (fcc)	700		520/300	**12**
Ag*	A1 (fcc)	460	16	300/200	**12**
Rh*	A1 (fcc)	460	16	300/200	**12**
Pd*	A1 (fcc)	460	16	300/200	**12**

energy and the bulk modulus of Na is very small. The influence on the atomization energy is with 30 meV moderate. For all considered test systems, except Na, inclusion of core states does not change the RPA lattice constants by more than 0.2%. A 0.2% change is observed for GaP and although we consider this difference to be acceptable we used the Ga_{3s3p} for all systems containing Ga (GaN, GaP, GaAs) in the following sections.

For all systems tested in this section, the effect of the core states on the atomization energies is of the order of 40 meV, and with 60 meV largest for Al. Considering that the RPA results in errors of several 100 meV in the atomization energies, this difference is small enough to justify the use of the frozen-core approximation. But it is possible that geometrical properties and atomization energies of other elements or other structures than considered here are more strongly effected by the use of the frozen-core approximation and tests will be necessary, if one aims at a very high accuracy.

III. RESULTS

A. Lattice constants and bulk moduli of solids

Tables V and VI summarize lattice constants and bulk moduli, respectively. The errors (%) with respect to the experimental values are visualized in Fig. 4 (lattice constants) and Fig. 5 (bulk moduli).

The experimental lattice constants have been corrected for zero-point anharmonic expansion effects. We have applied the quasiharmonic approximation, i.e., at a set of volumes the harmonic vibrational frequencies were accurately determined using *ab initio* calculations, and the zero-point ener-

TABLE IV. Influence of the core states on the KS-PBE and RPA lattice constants (Å) and atomization energies (eV/atom). In the second column the states treated as valence states are listed. Stars imply that this potential has been used in the following sections. In the last column, the energy of the highest core state, E_{core}, is given in eV with respect to the Fermi level.

		DFT-PBE		RPA		
	Valence	a_0	E_0	a_0	E_0	E_{core}
Na	$3s$	4.184	1.09	4.254	0.97	
Na^{*}_{2s2p}	$2s2p3s$	4.196	1.08	4.182	1.00	−25
Al^{*}	$3s3p$	4.035	3.44	4.037	3.22	
Al_{2s2p}	$2s2p3s3p$	4.039	3.42	4.033	3.28	−65
Si^{*}	$3s3p$	5.466	4.55	5.432	4.39	
Si_{2s2p}	$2s2p3s3p$	5.471	4.55	5.438	4.34	−90
Cu^{*}	$3d4s$	3.634	3.48	3.597	3.36	
Cu_{3p}	$3p3d4s$	3.640	3.48	3.599	3.37	−70
GaP	$3d4s4p$	5.508	3.47	5.429	3.51	
$\text{Ga}_{3s3p}\text{P}^{*}$	$3s3p3d4s4p$	5.507	3.48	5.442	3.48	−95

gies were added to the ground-state energies at each volume. More details about the calculation of phonon frequencies and density of states in the framework of VASP have been presented in Refs. 70 and 71. For the evaluation of the anharmonic expansion effect, we closely followed the procedure adopted in Ref. 71. More details about the technical settings applied in the calculations will be presented in a forthcoming paper.[72] The theoretical bulk moduli have not been corrected for zero-point vibration effects.

The presented lattice constants and bulk moduli have been obtained by a Birch-Murnaghan equation of state fitted to energies evaluated at seven volumes centered on the experimental value. If the error in the lattice constant was larger than 3%, additional points have been considered. PBE orbitals (and eigenenergies) have been used for the evaluation of the exact exchange energy E_{EXX} and the total RPA energy ($E_{\text{EXX}}+E_c^{\text{RPA}}$). For Si, C, and Cu, lattice constants and bulk moduli have additionally been calculated using LDA orbitals. The difference between EXX and RPA lattice constants obtained from LDA and PBE orbitals and one-electron energies is smaller than 0.1%.

Besides the exact exchange (EXX) and RPA lattice constants and bulk moduli, KS-DFT results based on the LDA and PBE functionals are presented in Tables V and VI. The LDA and PBE lattice constants and bulk moduli follow the well known trend: LDA lattice constants are too small, LDA bulk moduli too large, and the opposite applies to the PBE functional. For both functionals, errors become larger for ionic compounds. The overestimation of the PBE lattice constants tends to be additionally more pronounced for solids with heavier elements as can be observed for the series AlN-AlP-AlAs, as well as GaN-GaP-GaAs and InP-InAs-InSb.

For lattice constants and bulk moduli, the quality of the EXX only results depends on whether the material is an insulator/semiconductor or a metal. In the first case, the mean absolute relative error (MARE) of the EXX lattice constants is with 1.2% of the same order as for LDA and PBE (0.8% and 1.6%, respectively). But for metals, exact exchange only (MARE: 5.8%) performs significantly worse than the standard DFT functionals LDA and PBE (MARE 1.7% and 1.1%, respectively). Especially for simple metals without covalent bonding contributions, such as Na, Cu, and Ag, the EXX lattice constants are severely overestimated (10% for Cu and Ag, 7% for Na) and the errors in the bulk moduli reach up to ≈75% (Ag and Cu).

If the RPA correlation energy is included, lattice constants are overall (insulators, semiconductors, metals) in very good agreement with experiment (MARE: 0.4%) and outperform the PBE (MARE: 1.4%) and LDA (MARE: 1.0%). The large errors of the EXX lattice constants for Na, Cu, and Ag are drastically reduced (e.g., from 10% to 0.1% for Cu, and from 11% to 0.6% for Ag). RPA bulk moduli are improved compared to the PBE ones (4% versus 11%). Additionally, the errors in the RPA lattice constants do not increase from the light to the heavy elements, as opposed to PBE. For the series InP, InAs, InSb, the PBE error increases from 1.7 over 2.3 to 2.6%, while the RPA errors are with 0.2, 0.4, and 0.4% rather constant. The same applies for the series Si, C, and Ge, and GaN, GaP, and GaAs.

The good performance of the RPA for lattice constants and bulk moduli for such diverse materials as studied in this work suggests that the volume dependence of the total (correlation) energy is very well reproduced by the RPA, although absolute values of the RPA correlation energy are known to differ by more than 30% from the exact correlation energy.[23]

The RPA+ correction leads to an increase in the lattice constants and a decrease in the bulk moduli compared to RPA, increasing the error with respect to experiment. Typical changes from RPA to RPA+ amount to 0.2–0.3 % in the lattice constants. For Na the change is with 0.6% relatively large. The lattice constants are still in good agreement with experiment, but the MARE is slightly larger than for the RPA (0.4% → 0.6%).

Comparison with previous work is rather difficult, since the literature values show large scatter. For Si, other all-

TABLE V. Lattice constants in Å. The experimentally measured or extrapolated $T=0$ K lattice constants have been taken from Ref. 67 (see also references therein), except for AlN (Ref. 68) and InSb (Ref. 69). Errors of the theoretical lattice constants (%) are evaluated with respect to experimental values that are corrected for zero-point anharmonic effects. Zero-point vibration effects were determined by calculating the phonon dispersion relation at a set of volumes and calculating the zero-point vibrational energies (Refs. 70–72). Experimental uncorrected (parenthesis) and corrected lattice constants are summarized in the last columns. Italic letters refer to data obtained from DFT-LDA orbitals and eigenenergies. In all other cases, DFT-PBE input has been used for the evaluation of the EXX and RPA lattice constants.

	PBE		LDA		EXX		RPA		RPA+		Expt.	
Name	*a*	Error	*a*	Error	*a*	Error	*a*	Error	*a*	Error	corr.	uncorr.
C	3.569	0.5	3.534	−0.5	3.540	−0.4	3.572	0.5	3.578	0.7	3.553	(3.567)
C		LDA wave function			3.540	−0.4	3.574	0.6	3.580	0.8		
Si	5.466	0.8	5.404	−0.3	5.482	1.1	5.432	0.2	5.445	0.4	5.421	(5.430)
Si		LDA wave function			5.479	1.1	5.433	0.2	5.446	0.5		
Ge	5.765	2.1	5.627	−0.3	5.701	1.0	5.661	0.3	5.676	0.6	5.644	(5.652)
SiC	4.378	0.7	4.332	−0.3	4.351	0.1	4.365	0.4	4.374	0.6	4.346	(4.358)
AlN	4.397	0.7	4.344	−0.5	4.346	−0.5	4.394	0.6	4.402	0.8	4.368	(4.380)
AlP	5.501	0.9	5.435	−0.3	5.513	1.1	5.467	0.3	5.479	0.5	5.451	(5.460)
AlAs	5.727	1.4	5.630	−0.3	5.698	0.9	5.675	0.5	5.690	0.7	5.649	(5.658)
GaN	4.551	0.7	4.460	−1.3	4.485	−0.8	4.519	0.0	4.528	0.2	4.520	(4.531)
GaP	5.507	1.3	5.396	−0.8	5.519	1.5	5.442	0.1	5.456	0.3	5.439	(5.448)
GaAs	5.749	1.9	5.611	−0.5	5.706	1.2	5.661	0.4	5.675	0.6	5.640	(5.648)
InP	5.955	1.7	5.827	−0.5	5.940	1.4	5.867	0.2	5.882	0.4	5.858	(5.866)
InAs	6.184	2.3	6.029	−0.3	6.120	1.2	6.070	0.4	6.087	0.7	6.047	(6.054)
InSb	6.633	2.6	6.452	−0.2	6.585	1.8	6.494	0.4	6.514	0.7	6.468	(6.474)
MgO	4.259	1.7	4.169	−0.5	4.173	−0.4	4.225	0.9	4.233	1.1	4.189	(4.207)
LiF	4.069	2.4	3.913	−1.5	3.991	0.5	3.998	0.7	4.010	1.0	3.972	(4.010)
NaF	4.707	2.7	4.511	−1.5	4.614	0.7	4.625	0.9	4.635	1.2	4.582	(4.609)
LiCl	5.149	1.6	4.967	−2.0	5.272	4.0	5.074	0.1	5.091	0.4	5.070	(5.106)
NaCl	5.697	2.3	5.469	−1.8	5.778	3.8	5.588	0.3	5.607	0.7	5.569	(5.595)
Na	4.196	−0.4	4.056	−3.7	4.494	6.6	4.182	−0.8	4.208	−0.1	4.214	(4.225)
Al	4.035	0.4	3.983	−0.9	4.104	2.1	4.037	0.5	4.052	0.8	4.018	(4.032)
Cu	3.634	1.1	3.523	−2.0	3.968	10.4	3.597	0.1	3.606	0.3	3.595	(3.603)
Cu		LDA wave function			3.968	10.4	3.601	0.2	3.610	0.4		
Rh	3.824	0.8	3.753	−1.1	3.748	−1.2	3.811	0.4	3.819	0.7	3.794	(3.798)
Pd	3.935	1.5	3.830	−1.2	4.003	3.3	3.896	0.5	3.905	0.7	3.876	(3.881)
Ag	4.146	2.1	4.002	−1.5	4.507	11.0	4.087	0.6	4.098	0.9	4.062	(4.069)
MARE (%)	Metals	1.1		1.7		5.8		0.5		0.6		
	Insulators	1.6		0.8		1.2		0.4		0.6		
	All	1.4		1.0		2.4		0.4		0.6		

electron calculations found a very similar lattice constant of 5.45 Å,[41] whereas previous pseudopotential RPA calculations yield a lattice constant of 5.36 Å (Ref. 43) and 5.38 Å (Ref. 45). This might indicate that the pseudopotential approximation possibly yields too small lattice constants due to the neglect of core-valence exchange effects.

In summary, for the systems studied in this work, the RPA outperforms both the LDA and PBE with respect to lattice constants and bulk moduli. The RPA however tends to overestimate the lattice constants by approximately 0.4% if the experimental lattice constants are corrected for zero-point anharmonic expansion effects. Using either LDA or PBE orbitals as input seems to have hardly any influence on the lattice constants and bulk moduli.

B. Atomization energies of solids

RPA atomization energies of solids have only been presented very recently,[46] because the calculation of the atomic correlation energy requires rather large volumes in order to minimize the interaction between atoms in repeated supercells. Energy differences of finite systems, as required for the evaluation of molecular atomization energies, converge significantly faster with the volume considered. Furthermore,

TABLE VI. Bulk Moduli in GPa and relative error (%) with respect to the experimental bulk moduli in percent. Italic letters refer to data obtained from DFT-LDA orbitals and eigenenergies. In all other cases, DFT-PBE input has been used. The experimental bulk moduli are not corrected for zero-point vibration effects. All experimental bulk moduli, expect for AlN (Ref. 73), AlP and AlAs (Ref. 74), and InP, InAs, InSb, and Ge (Ref. 75) have been taken from Ref. 58.

		PBE		LDA		EXX		RPA		RPA+		
Name		*B*	Error	*B*	Error	*B*	Error	*B*	Error	*B*	Error	Expt.
C		434	−2	465	5	512	15	441	0	436	−2	443
C			LDA wave function			509	15	439	−1	433	−2	
Si		89	−10	97	−3	108	9	99	0	97	−2	99
Si			LDA wave function			108	9	98	−1	96	−3	
Ge		58	−23	72	−6	91	20	77	2	76	−1	76
SiC		212	−6	229	2	253	13	223	−1	220	−2	225
AlN		194	−4	211	5	240	19	200	−1	197	−3	202
AlP		83	−4	90	5	99	16	92	7	90	5	86
AlAs		67	−13	75	−2	86	11	77	0	75	−3	77
GaN		171	−19	201	−4	239	14	189	−10	186	−11	210
GaP		76	−14	90	1	96	8	87	−2	84	−5	89
GaAs		60	−21	74	−3	87	15	77	2	76	0	76
InP		59	−16	71	0	82	16	71	0	70	−2	71
InAs		49	−16	60	4	67	15	59	2	57	−1	58
InSb		37	−20	46	1	49	6	44	−5	42	−8	46
MgO		149	−10	172	5	196	19	168	2	166	1	165
LiF		68	−3	87	24	80	15	76	8	74	6	70
NaF		45	−11	61	20	54	5	53	4	52	1	51
LiCl		32	−9	41	17	30	−16	37	5	36	2	35
NaCl		24	−13	32	19	22	−17	29	7	28	4	27
Na		8	−3	9	15	5	−33	8	5	8	0	8
Al		77	−3	84	6	61	−23	77	−2	74	−6	79
Cu		138	−3	186	31	32	−78	153	8	149	5	142
Cu			LDA wave function			32	−77	152	7	148	4	
Rh		255	−5	317	18	322	20	258	−4	253	−6	269
Pd		162	−17	226	16	97	−50	181	−7	176	−10	195
Ag		90	−17	138	27	27	−75	105	−3	103	−6	109
MARE (%)	Metals		8		19		46		5		5	
	Insulators		12		7		14		3		3	
	All		11		10		22		4		4	

the calculation of the absolute correlation energies of solids requires a denser *k*-point grid than the evaluation of the lattice constants.

Before discussing the atomization energies obtained within the RPA, it should be kept in mind that total RPA correlation energies possess errors of the order of 30%. This applies to extended systems (for the UEG, see Refs. 18, 21, and 23 and references therein) as well as to atoms.[22] The RPA+ correction leads to improved total energies, however, energy differences (atomization energies) are even slightly worse than using the uncorrected RPA energies (see also Ref. 24). This agrees with our observation, that lattice constants using RPA+ are worse than those obtained using the RPA (see Table V).

In Table VII, atomization energies using the exact exchange only and the RPA energy (exact exchange energy plus RPA correlation energy) are presented. PBE orbitals and eigenenergies have been used throughout for the evaluation of the EXX and RPA atomization energies. Again, LDA and PBE atomization energies are given for comparison. In Fig. 6, the percentage of the total experimental atomization energy that is obtained using the PBE, EXX only, and the RPA is shown.

Absolute atomization energies evaluated using the LDA exchange-correlation energy functional are consistently overestimated. The mean average error is 0.7 eV/atom or 18% of the experimental value. The generalized gradient approximation, as applied in the PBE functional, cures large parts of this error and the mean absolute relative error using the PBE exchange-correlation energy reduces to 0.2 eV or 5%. Although PBE does not provide chemical accuracy (1 kcal/mol≈43 meV), errors are of the same order for

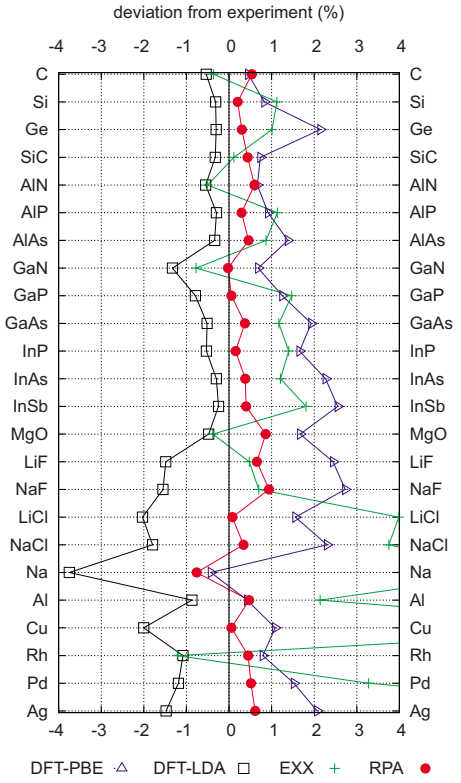

FIG. 4. (Color online) Relative error (%) of the theoretical lattice constants with respect to experiment.

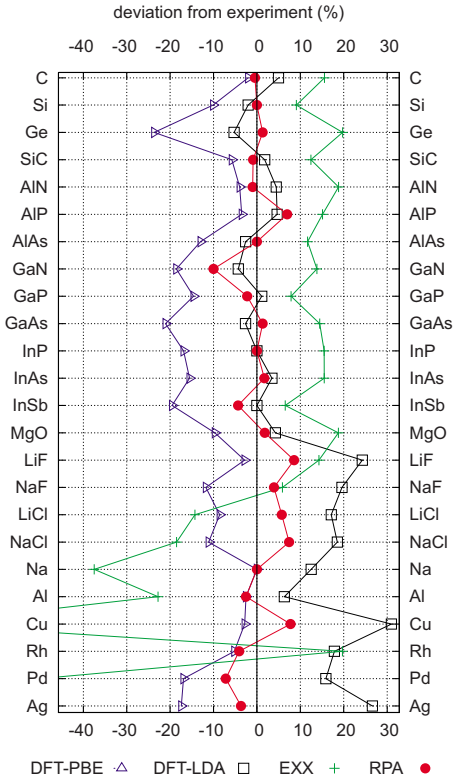

FIG. 5. (Color online) Relative error (%) of the theoretical bulk moduli with respect to experiment.

metals and insulators, covalent and ionic systems, and DFT-PBE therefore guarantees a well balanced compromise for many applications. Interestingly DFT-PBE does not perform well for heats of formation with respect to constituents in the respective ground state at ambient conditions (e.g. Mg-metal$+O_2/2 \rightarrow$MgO),[46] which is in most cases related to the fact that atomization energies of small molecules tend to be overestimated, while atomization energies of solids are underestimated, resulting in too small absolute heats of formation for solids.

In contrast to PBE, the quality of the EXX atomization energies depends on whether the considered solid is a metal or an insulator. While, due to the lack of correlation, the absolute EXX atomization energies are too small for all solids, the average error for metals (3.8 eV/atom or 100%) is significantly larger than the error for insulators and semiconductors (1.7 eV/atom or 41%). Two extreme cases are Rh and Pd, where EXX predicts that isolated atoms are more stable than the metallic solid.

When adding the RPA correlation energy, the largest part of the experimental atomization energy (in average 94% for the considered insulators and semiconductors, 90% for the metals) is recovered (see Fig. 6). For all considered materials, the atomization energy is underestimated, with errors of the order of 0.2–0.5 eV/atom. This error is very similar to the one found by Furche[24] for the atomization energies of molecules. The RPA+correction, which should provide a better description of the short-range correlation, does not improve the atomization energies. In general, the absolute atomization energy decreases with respect to the RPA values (by $\approx$60 meV), so that the binding is even more underestimated than in the RPA.

Finally, we would like to discuss the influence of the initial orbitals and one-electron energies on the atomization energy (see Table VIII). For the lattice constants and bulk moduli, we have found very similar results for PBE and LDA input. For many systems, however, this does not hold for the atomization energies. The main issue is the energy of the atom: PBE favors a nonspherical solution for most atoms, whereas LDA favors a spherical solution, e.g., for carbon 2 electrons are distributed over the 3*p* orbitals in LDA resulting in fractional occupancies of 2/3. As a result, the energy of the atom is very different for PBE and LDA orbitals. We found that RPA is sensitive to whether the atom is spherical or nonspherical, which might well reflect an intrinsic failure of the RPA.[39] For the present work, we adopted the pragmatic solution, to calculate all atomization energies with respect to the symmetry broken, nonspherical atom (PBE solution).

For cases, where LDA and PBE favor the same atomic solution, as well as for relative energies between solids, the initial orbitals have little influence on energy differences. This is demonstrated for the atomization energy of Cu (one *s* electron) and the heat of formation of the reaction

$$\text{C(diamond)} + \text{Si(diamond)} \rightarrow \text{SiC(zinc-blende)}$$

in Table VIII.

TABLE VII. Atomization energies and absolute errors with respect to zero-point vibrational energy corrected experimental values (eV/atom). For all solids, except for Ge, AlN, AlP, and AlAs (Ref. 76), and InP, InAs, and InSb (Ref. 77) experimental values are taken from Ref. 58. DFT-PBE orbitals and eigenenergies have been used as input for the EXX and RPA-ACFD calculations.

		PBE		LDA		EXX		RPA		RPA+		Expt.	Expt.
Name		*E*	Error	*E*	Error	*E*	Error	*E*	Error	*E*	Error	Corr.	Uncorr.
C		7.72	0.16	9.01	1.46	5.18	−2.36	7.00	−0.55	6.93	−0.62	7.55	(7.37)
Si		4.55	−0.13	5.34	0.66	2.82	−1.86	4.39	−0.29	4.33	−0.35	4.68	(4.62)
Ge		3.71	−0.20	4.62	0.71	1.95	−1.97	3.59	−0.33	3.53	−0.38	3.92	(3.88)
SiC		6.40	−0.08	7.45	0.97	4.36	−2.12	6.04	−0.44	5.96	−0.52	6.48	(6.37)
AlN		5.72	−0.14	6.68	0.82	3.65	−2.21	5.46	−0.39	5.39	−0.47	5.85	(5.76)
AlP		4.09	−0.22	4.87	0.56	2.53	−1.79	4.07	−0.24	4.02	−0.30	4.32	(4.26)
AlAs		3.69	−0.13	4.52	0.70	2.15	−1.67	3.67	−0.16	3.61	−0.21	3.82	(3.78)
GaN		4.37	−0.18	5.46	0.91	2.22	−2.34	4.23	−0.32	4.17	−0.39	4.55	(4.48)
GaP		3.48	−0.13	4.39	0.79	1.83	−1.77	3.48	−0.13	3.46	−0.15	3.61	(3.56)
GaAs		3.14	−0.20	4.09	0.74	1.51	−1.84	3.14	−0.21	3.09	−0.26	3.34	(3.31)
InP		3.14	−0.33	4.15	0.68	1.56	−1.91	3.12	−0.35	3.07	−0.40	3.47	(3.43)
InAs		2.88	−0.20	3.80	0.72	1.31	−1.77	2.85	−0.23	2.80	−0.28	3.08	(3.05)
InSb		2.63	−0.18	3.50	0.69	1.10	−1.71	2.59	−0.22	2.55	−0.26	2.81	(2.79)
MgO		4.98	−0.23	5.88	0.67	3.47	−1.73	4.91	−0.29	4.83	−0.37	5.20	(5.13)
LiF		4.33	−0.13	4.94	0.48	3.25	−1.21	4.20	−0.26	4.15	−0.31	4.46	(4.40)
NaF		3.82	−0.16	4.38	0.40	2.79	−1.18	3.77	−0.21	3.71	−0.26	3.97	(3.93)
LiCl		3.37	−0.21	3.83	0.25	2.68	−0.90	3.36	−0.23	3.31	−0.27	3.59	(3.55)
NaCl		3.10	−0.24	3.50	0.16	2.54	−0.80	3.15	−0.19	3.11	−0.23	3.34	(3.31)
Na		1.08	−0.04	1.26	0.14	0.23	−0.90	1.00	−0.12	0.98	−0.14	1.12	(1.11)
Al		3.44	0.01	4.04	0.61	1.33	−2.10	3.22	−0.21	3.14	−0.29	3.43	(3.39)
Cu		3.48	−0.04	4.55	1.02	0.03	−3.50	3.36	−0.16	3.30	−0.22	3.52	(3.49)
Rh		5.74	−0.04	7.67	1.89	−2.88	−8.67	5.05	−0.74	4.97	−0.81	5.78	(5.75)
Pd		3.74	−0.20	5.08	1.15	−1.26	−5.20	3.41	−0.53	3.35	−0.59	3.94	(3.91)
Ag		2.52	−0.46	3.64	0.66	0.52	−2.46	2.64	−0.35	2.58	−0.41	2.98	(2.96)
MAE (eV/atom)	Metals	0.13		0.91		3.80		0.35		0.41			
	Insulator	0.18		0.69		1.73		0.28		0.34			
	All	0.17		0.74		2.25		0.30		0.35			
MARE (%)	Metals	4		24		101		10		12			
	Insulator	5		16		41		6		8			
	All	5		18		56		7		9			

IV. DISCUSSION

In this work, we have evaluated lattice constants, bulk moduli, and atomization energies of 24 solids by combining the exact exchange energy with a compatible correlation energy calculated within the random phase approximation (both evaluated at DFT orbitals). From a theoretical point of view, the most important result of our study is a generalization of the total RPA correlation energy to systems with partially filled states. We have shown that this requires a careful treatment of fractional occupancies in both the exchange and correlation energy. Specifically, we found that the exchange energy needs to be modified to properly take into account fractionally filled orbitals (see Sec. II D).

From a practical point, we have demonstrated that the RPA yields excellent lattice constants and good relative energies. Before this work, the evaluation of RPA lattice constants has been restricted to few test cases: h-BN,[42] Si,[41,43] Na,[41] NaCl,[43] rare-gas solids,[38] and the benzene crystal.[44] Most of these calculations have been performed using the pseudopotential approximation, which makes very accurate predictions difficult. In this and a previous work,[46] we found that the RPA predicts accurate lattice constants and bulk moduli for insulators and semiconductors, as well as, metals. If experimental lattice constants are corrected for zero-point vibration effects, as done in the present work, the RPA leads to a slight overall overestimation of the binding lengths [mean absolute relative error (MARE) of 0.4%]. The error in the lattice constants is smaller than for the PBE (MARE: 1.4%) or LDA (MARE: 1.0%) and is comparable to the PBEsol (Ref. 78) error (for PBEsol results see, e.g., Ref. 67). In contrast to the latter, the RPA correlation energy is fully nonlocal and is capable of describing van der Waals bonded systems reasonably well.[38,42,44,46] In particular, we note that

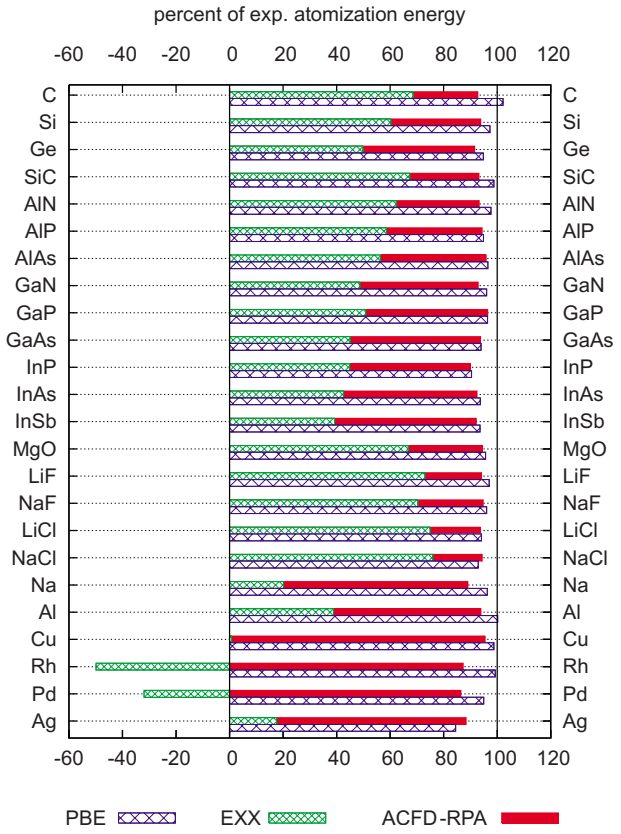

FIG. 6. (Color online) Percentage of experimental, zero-point energy corrected, atomization energy.

the error in the lattice constants does not increase with increasing mass of the constituents, as found for PBE or PBEsol. For the systems considered in the present work, the RPA additionally performs well for the prediction of bulk moduli, with a MARE of 4%, which is again smaller than for both PBE (11%) and LDA (10%). As the RPA energies are evaluated non-self-consistently by calculating the exact exchange energy and the RPA correlation energy using DFT orbitals and eigenenergies, the dependence on the applied functional has been tested by using both, LDA and PBE input. The effect on lattice constants and bulk moduli was found to be very small.

We also presented results for the atomization energies of solids. These calculations are technically rather challenging using plane waves, since the computational complexity is cubic with the supercell volume. The RPA atomization energies of 24 systems, ranging from covalent over ionic to metallic materials, have been presented in Sec. III B. The atomization energies exhibit errors of the order of 0.2–0.5 eV evaluated with respect to the zero-point corrected experimental energies, and the errors are larger than using the PBE (but still significantly smaller than using the LDA). This is certainly disappointing, in particular considering that the evaluation of the RPA atomization energies is much more time-consuming than a standard LDA or PBE calculation. However, the RPA atomization energies are consistently too small, and errors cancel largely in heats of formation, as we have shown in Ref. 46. Such systematic error cancellation was not observed for PBE. As for the lattice constants and bulk moduli, we tested the influence of the functional applied for the evaluation of the input orbitals and eigenenergies. Again we found little influence, except in those cases, where PBE and LDA predict different ground states for the atoms (spherical versus nonspherical).

An open issue is whether an evaluation of the total energy using self-consistent RPA orbitals will change the results presented here. The preferred pathway towards self-consistency is via the solution of the Sham and Schlüter equation,[79] which yields an effective multiplicative Kohn-Sham potential (in the following referred to as RPA-KS). For solids, the calculations presented so far (Si, C, GaAs, AlAs, LiF, Ar) (Refs. 80–83) suggest that the RPA-KS potential exhibits only small differences to the LDA or PBE potentials, suggesting that self-consistency is a minor issue for extended systems. This conclusion was also confirmed by Kotani,[84] who evaluated the RPA potentials of Cu, Ni, Fe, and Co using a static approximation to the dielectric function. However, for atoms and molecules, the LDA and PBE potentials are known to miss the leading $1/r$ dependence of the potential at large distances from the nuclei, in contrast to the exact and RPA-KS potential.[55] This will possibly change atomiza-

TABLE VIII. Dependence of the Cu atomization energies and of the SiC heat of formation on the applied orbitals and eigenenergies (DFT-PBE or DFT-LDA). Total energies obtained from EXX only (EXX) and the EXX+RPA correlation (RPA), the difference yielding the atomization energy per atom (eV/atom) and the heats of formation per formula unit (eV/SiC), respectively, are presented.

Cu atomization energy: Cu_{bulk}-Cu_{atom}						
	E_{bulk}^{EXX}	E_{atom}^{EXX}	E_{bulk}^{RPA}	E_{atom}^{RPA}	ΔE^{EXX}	ΔE^{RPA}
PBE	−3.07	−3.05	−18.28	−14.92	−0.03	−3.36
LDA	−2.98	−2.97	−18.25	−14.90	−0.01	−3.35

SiC heats of formation: SiC_{bulk}-(Si_{bulk}+C_{bulk})						
	E_{SiC}^{EXX}	$E_{(Si+C)}^{EXX}$	E_{SiC}^{RPA}	$E_{(Si+C)}^{RPA}$	ΔE^{EXX}	ΔE^{RPA}
PBE	−28.72	−28.00	−41.79	−41.12	−0.72	−0.66
LDA	−28.61	−27.89	−41.73	−41.07	−0.72	−0.66

tion energies. Only a self-consistent treatment of the RPA will allow a final answer to whether the errors in atomization energies are related to the used orbitals or are intrinsic to the RPA.

Although the RPA provides a well balanced description of lattice constants and heats of formation for the systems studied in this work, several shortcomings of the RPA need to be addressed in future work. From a practical point of view, RPA calculations require the evaluation of the response function. This makes RPA calculations much slower than standard DFT calculations. For large van der Waals bonded systems, there is hardly any choice but accounting for van der Waals interactions using pair-wise additive potentials (see, e.g., Ref. 85) or approximative nonlocal correlation energy functionals as proposed by Langreth and Lundquist.[86]

From a fundamental point of view, the RPA is a quite crude approximation to the "true" correlation energy. Two obvious exemplifications of the approximate nature of the RPA are its failure to describe dissociation curves of small charged or uncharged molecules[39] and the correlation energy error for the uniform electron gas. For the UEG the absolute RPA correlation energies are overestimated by more than 30% (see e.g. Refs. 18 and 21), and the same overestimation is observed for atoms and small molecules.[22] To remedy this, Kurth and Perdew proposed a correction term for the short-range RPA error using a local or semilocal approximation.[20] Per definition, this RPA+ method provides the exact correlation energy for the uniform electron gas and also cancels large parts of the RPA correlation error for atoms.[22] Unfortunately, the improvements in the absolute correlation energies do not transfer to correlation energy differences. This has been first observed by Furche[24] for atomization energies of small molecules, and is confirmed in the present work for the lattice constants and atomization energies of solids. On the contrary, the RPA+ enhances the existing tendencies of the RPA to overestimate the lattice constants (from MARE 0.4% to 0.6%) and underestimate the atomization energies (MAE 0.30 eV/atom to 0.35 eV/atom).

Improvements over RPA can be constructed both in the framework of the adiabatic connection fluctuation-dissipation theorem by an inclusion of an exchange-correlation kernel in the Dyson equation or in the framework of coupled cluster theory.[18,19,23] The first approach has already been tested to some extend for molecular systems[32,34] and the uniform electron gas.[29,30,43] Calculations for the uniform electron gas[29] emphasize the importance of the nonlocality of the exchange-correlation kernel, while the frequency dependence seems to be of minor importance. Calculations of jellium clusters performed in Ref. 43 suggest that the static energy-optimized nonlocal Hubbard-like (OHU) kernel proposed by Jung and coworkers[87] outperforms the RPA+ slightly, whereas the Petersilka-Gossman-Gross (PGG) functional[88] results in larger errors. The inclusion of approximate exchange-correlation kernels will probably be one of the next steps in the investigation of ACFD correlation energies for solids.

Alternative methods for improving the RPA correlation energy are related to coupled cluster theory. The RPA approximates the correlation energy as a summation over ring diagrams; exchange like diagrams of higher orders are not included, which is the main reason for the observed overestimation of the absolute correlation energies and a nonvanishing correlation energy of one-electron systems (self-correlation error). A possible route to lift this short comings is the inclusion of the second-order screened exchange (SOSEX) diagram.[18,23] In a recent work we could show that this approximation improves the absolute correlation energy as well as correlation energy differences resulting in improved lattice constants and atomization energies,[23] but unfortunately this approximation does not improve reaction barriers or the dissociation curves of small uncharged molecules.[89]

V. CONCLUSION

From today's point of view, we feel that the RPA is a practicable method for systems up to 100 atoms. It provides excellent lattice constants, bulk moduli, and very good heats of formation, as well as, adsorption and surface energies. Furthermore it seamlessly incorporates van der Waals bonding, something that very few other methods do. In particular for metals, it seems the only method for a systematic improvement over conventional semilocal functionals. Since forces are not yet available, RPA needs to rely on good geometries, but fortunately, semilocal functionals perform quite well in this respect. The RPA is ideally suited to obtain a second "opinion," one that goes beyond the semilocal approximation and includes more of the important physics. Specifically, nonlocal screened exchange is included in a nonempirical manner, and long-range dynamic correlation effects are accounted for.

ACKNOWLEDGMENTS

This work was supported by the Austrian Fonds zur Förderung der wissenschaftlichen Forschung (FWF) under Grant No. Y218 (START) and Project No. W4.

*judith.harl@univie.ac.at

[1] W. Kohn and L. J. Sham, Phys. Rev. **140**, A1133 (1965).
[2] J. P. Perdew, K. Burke, and M. Ernzerhof, Phys. Rev. Lett. **77**, 3865 (1996).
[3] J. P. Perdew, Int. J. Quantum Chem. **48**, 93 (1993).
[4] J. P. Perdew, M. Ernzerhof, and K. Burke, J. Chem. Phys. **105**, 9982 (1996).
[5] J. Paier, R. Hirschl, M. Marsman, and G. Kresse, J. Chem. Phys. **122**, 234102 (2005).
[6] J. Paier, M. Marsman, K. Hummer, G. Kresse, I. C. Gerber, and J. G. Ángyán, J. Chem. Phys. **124**, 154709 (2006).
[7] J. Heyd and G. E. Scuseria, J. Chem. Phys. **121**, 1187 (2004).

[8] S. Casassa, M. Halo, L. Maschio, C. Roetti, and C. Pisani, Theor. Chem. Acc. **117**, 781 (2007).
[9] M. Marsman, A. Grüneis, J. Paier, and G. Kresse, J. Chem. Phys. **130**, 184103 (2009).
[10] A. Grüneis, M. Marsman, and G. Kresse (unpublished).
[11] for a overview see B. Paulus, Phys. Rep. **428**, 1 (2006).
[12] D. C. Langreth and J. P. Perdew, Solid State Commun. **17**, 1425 (1975).
[13] O. Gunnarsson and B. I. Lundqvist, Phys. Rev. B **13**, 4274 (1976).
[14] D. C. Langreth and J. P. Perdew, Phys. Rev. B **15**, 2884 (1977).
[15] E. Runge and E. K. U. Gross, Phys. Rev. Lett. **52**, 997 (1984).
[16] E. K. U. Gross and W. Kohn, Phys. Rev. Lett. **55**, 2850 (1985).
[17] A. Klein, Phys. Rev. **121**, 950 (1961).
[18] D. L. Freeman, Phys. Rev. B **15**, 5512 (1977).
[19] G. E. Scuseria, T. M. Henderson, and D. C. Sorensen, J. Chem. Phys. **129**, 231101 (2008).
[20] S. Kurth and J. P. Perdew, Phys. Rev. B **59**, 10461 (1999).
[21] J. P. Perdew and Y. Wang, Phys. Rev. B **45**, 13244 (1992).
[22] H. Jiang and E. Engel, J. Chem. Phys. **127**, 184108 (2007).
[23] A. Grüneis, M. Marsman, J. Harl, L. Schimka, and G. Kresse, J. Chem. Phys. **131**, 154115 (2009).
[24] F. Furche, Phys. Rev. B **64**, 195120 (2001).
[25] U. von Barth and L. Hedin, J. Phys. C **5**, 1629 (1972).
[26] J. Harris and A. Griffin, Phys. Rev. B **11**, 3669 (1975).
[27] J. M. Pitarke and A. G. Eguiluz, Phys. Rev. B **57**, 6329 (1998).
[28] J. F. Dobson and J. Wang, Phys. Rev. Lett. **82**, 2123 (1999).
[29] M. Lein, E. K. U. Gross, and J. P. Perdew, Phys. Rev. B **61**, 13431 (2000).
[30] R. Asgari, M. Polini, B. Davoudi, and M. P. Tosi, Phys. Rev. B **68**, 235116 (2003).
[31] N. E. Dahlen, R. van Leeuwen, and U. von Barth, Int. J. Quantum Chem. **101**, 512 (2005).
[32] M. Fuchs and X. Gonze, Phys. Rev. B **65**, 235109 (2002).
[33] M. Fuchs, Y. M. Niquet, X. Gonze, and K. Burke, J. Chem. Phys. **122**, 094116 (2005).
[34] F. Furche and T. Voorhis, J. Chem. Phys. **122**, 164106 (2005).
[35] F. Aryasetiawan, T. Miyake, and K. Terakura, Phys. Rev. Lett. **88**, 166401 (2002).
[36] N. E. Dahlen and U. von Barth, Phys. Rev. B **69**, 195102 (2004).
[37] N. E. Dahlen, R. van Leeuwen, and U. von Barth, Phys. Rev. A **73**, 012511 (2006).
[38] J. Harl and G. Kresse, Phys. Rev. B **77**, 045136 (2008).
[39] P. Mori-Sánchez, A. J. Cohen, and W. Yang, arXiv:0903.4403 (unpublished).
[40] J. Toulouse, I. C. Gerber, G. Jansen, A. Savin, and J. G. Ángyán, Phys. Rev. Lett. **102**, 096404 (2009).
[41] T. Miyake, F. Aryasetiawan, T. Kotani, M. van Schilfgaarde, M. Usuda, and K. Terakura, Phys. Rev. B **66**, 245103 (2002).
[42] A. Marini, P. García-González, and A. Rubio, Phys. Rev. Lett. **96**, 136404 (2006).
[43] P. García-González, J. J. Fernández, A. Marini, and A. Rubio, J. Phys. Chem. A **111**, 12458 (2007).
[44] D. Lu, Y. Li, D. Rocca, and G. Galli, Phys. Rev. Lett. **102**, 206411 (2009).
[45] H.-V. Nguyen and S. de Gironcoli, Phys. Rev. B **79**, 115105 (2009).
[46] J. Harl and G. Kresse, Phys. Rev. Lett. **103**, 056401 (2009).
[47] M. Rohlfing and T. Bredow, Phys. Rev. Lett. **101**, 266106 (2008).
[48] X. Ren, P. Rinke, and M. Scheffler, Phys. Rev. B **80**, 045402 (2009).
[49] G. Kresse and J. Hafner, Phys. Rev. B **48**, 13115 (1993).
[50] G. Kresse and J. Furthmüller, Comput. Mater. Sci. **6**, 15 (1996).
[51] P. E. Blöchl, Phys. Rev. B **50**, 17953 (1994).
[52] G. Kresse and D. Joubert, Phys. Rev. B **59**, 1758 (1999).
[53] M. Gajdoš, K. Hummer, G. Kresse, J. Furthmüller, and F. Bechstedt, Phys. Rev. B **73**, 045112 (2006).
[54] M. Shishkin and G. Kresse, Phys. Rev. B **74**, 035101 (2006).
[55] Y. M. Niquet, M. Fuchs, and X. Gonze, Phys. Rev. A **68**, 032507 (2003).
[56] S. L. Adler, Phys. Rev. **126**, 413 (1962).
[57] N. Wiser, Phys. Rev. **129**, 62 (1963).
[58] J. Paier, M. Marsman, and G. Kresse, J. Chem. Phys. **127**, 024103 (2007).
[59] A. E. Mattsson, R. Armiento, J. Paier, G. Kresse, J. M. Wills, and T. R. Mattson, J. Chem. Phys. **128**, 084714 (2008).
[60] J. P. Perdew and A. Zunger, Phys. Rev. B **23**, 5048 (1981).
[61] J. P. Perdew, A. Ruzsinszky, G. I. Csonka, O. A. Vydrov, G. E. Scuseria, V. N. Staroverov, and J. Tao, Phys. Rev. A **76**, 040501(R) (2007).
[62] M. E. Casida, in *Recent Advances in Density Functional Methods*, edited by D. P. Chong (World Scientific, Singapore, 1995), Vol. 1.
[63] F. Gygi and A. Baldereschi, Phys. Rev. B **34**, 4405 (1986).
[64] J. Spencer and A. Alavi, Phys. Rev. B **77**, 193110 (2008).
[65] J. Harl, G. Kresse, L. D. Sun, M. Hohage, and P. Zeppenfeld, Phys. Rev. B **76**, 035436 (2007).
[66] M. Methfessel and A. T. Paxton, Phys. Rev. B **40**, 3616 (1989).
[67] P. Haas, F. Tran, and P. Blaha, Phys. Rev. B **79**, 085104 (2009).
[68] A. Trampert, O. Brandt, and K. H. Ploog, in *Crystal Structure of Group III Nitrides*, Semiconductors and Semimetals Vol. 50, edited by J. I. Pankove and T. D. Moustakas (Academic, San Diego, 1998).
[69] O. Madelung, *Semiconductors: Basic Data* (Springer, Berlin, 1996).
[70] G. Kresse, J. Furthmüller, and J. Hafner, Europhys. Lett. **32**, 729 (1995).
[71] G. Kern, G. Kresse, and J. Hafner, Phys. Rev. B **59**, 8551 (1999).
[72] L. Schimka, J. Harl, and G. Kresse (unpublished).
[73] M. E. Sherwin and T. J. Drummond, J. Appl. Phys. **69**, 8423 (1991).
[74] S. B. Zhang and M. L. Cohen, Phys. Rev. B **35**, 7604 (1987).
[75] *Landolt-Börnstein Semiconductors*, edited by O. Madelung, U. Rössler, and M. Schulz (Springer-Verlag, Berlin, 2002), Vols. 41A1b and 41A1a.
[76] W. A. Harrison, *Electronic Structure and the Properties of Solids* (Dover, New York, 1989).
[77] T. Soma, J. Phys. C **11**, 2669 (1978).
[78] J. P. Perdew, A. Ruzsinszky, G. I. Csonka, O. A. Vydrov, G. E. Scuseria, L. A. Constantin, X. Zhou, and K. Burke, Phys. Rev. Lett. **100**, 136406 (2008).
[79] L. J. Sham and M. Schlüter, Phys. Rev. Lett. **51**, 1888 (1983).
[80] R. W. Godby, M. Schlüter, and L. J. Sham, Phys. Rev. Lett. **56**, 2415 (1986).
[81] R. W. Godby, M. Schlüter, and L. J. Sham, Phys. Rev. B **37**, 10159 (1988).
[82] M. Grüning, A. Marini, and A. Rubio, J. Chem. Phys. **124**, 154108 (2006).

[83] R. W. Godby, M. Schlüter, and L. J. Sham, Phys. Rev. B **36**, 6497 (1987).
[84] T. Kotani, J. Phys.: Condens. Matter **10**, 9241 (1998).
[85] S. Grimme, J. Comput. Chem. **27**, 1787 (2006).
[86] M. Dion, H. Rydberg, E. Schröder, D. C. Langreth, and B. I. Lundqvist, Phys. Rev. Lett. **92**, 246401 (2004).
[87] J. Jung, P. García-González, J. F. Dobson, and R. W. Godby, Phys. Rev. B **70**, 205107 (2004).
[88] M. Petersilka, U. J. Gossmann, and E. K. U. Gross, Phys. Rev. Lett. **76**, 1212 (1996).
[89] J. Paier, B. G. Janesko, T. M. Henderson, G. E. Scuseria, A. Grüneis, and G. Kresse, J. Chem. Phys. **132**, 094103 (2010).